Phase Transitions in the $LiNi_{0.5}Mn_{0.5}O_2$ System with Temperature

Yoyo Hinuma, Ying S. Meng, Kisuk Kang, and Gerbrand Ceder*

Massachusetts Institute of Technology, 77 Massachusetts Avenue, Cambridge, Massachusetts 02139

We investigate the phase transformations of layered $LiNi_{0.5}Mn_{0.5}O_2$ at finite temperature with a combined computational and experimental approach. The detailed changes in the ionic configurations with temperature are investigated by Monte Carlo simulations on the basis of a coupled cluster expansion that describes the dependence of the energy on the arrangement of Li^+, Ni^{2+}, and Mn^{4+} in the lithium layer and transition metal layer. First-principles energies in the GGA+U approximation were used to fit the Hamiltonian, as we find that GGA+U better represents magnetic interactions than standard GGA. The simulation results suggest two phase-transition temperatures at approximately 550 and 620 °C. Below the first phase-transition temperature, a structure with almost no Li/Ni disorder in the Li layer is energetically favorable. Between the two temperatures, a partially disordered flower structure with about 8−11% Li/Ni disorder is found. Above the second phase transition, a structure that is more disordered but still consistent with a $\sqrt{3} \times \sqrt{3}$ honeycomb model with 8−11% Li/Ni disorder is stable. The results from these simulations are corroborated with DSC, TEM, and XRD measurements on a recently synthesized $LiNi_{0.5}Mn_{0.5}O_2$ with negligible Li/Ni disorder.

Introduction

$LiNi_{0.5}Mn_{0.5}O_2$[1−6] is an interesting material in both its engineering and scientific aspects. The theoretical capacity of $LiNi_{0.5}Mn_{0.5}O_2$ as a cathode material in rechargeable Li batteries is about 280 mA h g^{-1}, of which 200 mA h g^{-1} can now routinely be achieved at low rates.[2−5] This is considerably higher than what is achieved with conventional $LiCoO_2$ (practical capacity about 150mAh/g). Moreover, because $LiNi_{0.5}Mn_{0.5}O_2$ does not contain the rather expensive cobalt, a reduction in cost for Li batteries may be realized with this material. Other properties of the material, such as thermal stability and safety, have also been demonstrated to be better than those of $LiCoO_2$.[2,4]

Although the rate capability of the material has generally been shown to be poor, recent structural modifications[6] indicate that it may be possible to overcome them, making this material even more attractive as a new electrode material. Much of the desirable properties are derived from the synergetic combination of Mn^{4+} and Ni^{2+}. Mn^{4+} is one of the most stable octahedral ions and will stabilize the structure when Li is extracted, whereas Ni^{2+} can be fully oxidized to Ni^{4+}, thereby compensating for the fact that Mn^{4+} cannot be oxidized.[7−10]

Although the average cation positions of $LiNi_{0.5}Mn_{0.5}O_2$ form an O3-type layered structure[11] similar to that of $LiCoO_2$, characterizing the more detailed cation ordering has been difficult.[3,12−18] In addition, a significant dependence of structure (and performance) on synthesis conditions exists: a small amount of Ni in the lithium layers is always observed in materials synthesized with conventional solid-state processes at temperatures around 900−1000 °C. In most cases, there is about 8−11% of such Li/Ni disorder.[2,14,15,19−23] Some literature suggests that Li/Ni disorder tends to slightly increase with decreasing annealing temperature.[4,19]

The valences of Ni and Mn are observed to be +2 and +4 respectively, both in computation[23] and X-ray absorption spectroscopy.[24,25] Thus, electrostatic interactions are likely

* Corresponding author. E-mail: gceder@mit.edu.
(1) Spahr, M. E.; Novak, P.; Haas, O.; Nesper, R. *J. Power Sources* **1997**, *68*, 629.
(2) Ohzuku, T.; Makimura, Y. *Chem. Lett.* **2001**, 744.
(3) Makimura, Y.; Ohzuku, T. *J. Power Sources* **2003**, *119*, 156.
(4) Lu, Z. H.; Beaulieu, L. Y.; Donaberger, R. A.; Thomas, C. L.; Dahn, J. R. *J. Electrochem. Soc.* **2002,** *149*, A778.
(5) Lu, Z. H.; MacNeil, D. D.; Dahn, J. R. *Electrochem. Solid State Lett.* **2001**, *4*, A191.
(6) Kang, K.; Meng, Y. S.; Breger, J.; et al. *Science* **2006**, *311*, 977.
(7) Reed, J.; Ceder, G. *Chem. Rev.* **2004**, *104*, 4513.
(8) Reed, J.; Ceder, G.; Van Der Ven, A. *Electrochem. Solid State Lett.* **2001**, *4*, A78.
(9) Kang, K.; Carlier, D.; Reed, J.; Arroyo, E. M.; Ceder, G.; Croguennec, L.; Delmas, C. *Chem. Mater.* **2003**, *15*, 4503.
(10) Kang, K.; Chen, C. H.; Hwang, B. J.; Ceder, G. *Chem. Mater.* **2004**, *16*, 2685.
(11) Delmas, C.; Fouassier, C.; Hagenmuller, P. *Physica B* **1980**, *99*, 81.
(12) Arachi, Y.; Kobayashi, H.; Emura, S.; Nakata, Y.; Tanaka, M.; Asai, T.; Sakaebe, H.; Tatsumi, K.; Kageyama, H. *Solid State Ionics* **2005**, *176*, 895.
(13) Islam, M. S.; Davies, R. A.; Gale, J. D. *Chem. Mater.* **2003**, *15*, 4280.
(14) Meng, Y. S.; Ceder, G.; Grey, C. P.; Yoon, W. S.; Shao-Horn, Y. *Electrochem. Solid State Lett.* **2004**, *7*, A155.
(15) Meng, Y. S.; Ceder, G.; Grey, C. P.; Yoon, W. S.; Jiang, M.; Breger, J.; Shao-Horn, Y. *Chem. Mater.* **2005**, *17*, 2386.
(16) Van der Ven, A.; Ceder, G. *Electrochem. Commun.* **2004**, *6*, 1045.
(17) Breger, J.; Dupre, N.; Chupas, P. J.; Lee, P. L.; Proffen, Th.; Parise, J. B.; Grey, C. P. *J. Am. Chem. Soc.* **2005**, *127*, 7529.
(18) Kobayashi, H.; Arachi, Y.; Kageyama, H.; Tatsumi, K. *J. Mater. Chem.* **2004**, *14*, 40.
(19) Lu, Z. H.; Chen, Z. H.; Dahn, J. R. *Chem. Mater.* **2003**, *15*, 3214.
(20) Lu, Z.; MacNeil, D. D.; Dahn, J. R. *Electrochem. Solid State Lett.* **2001**, *4*, A200.
(21) Yoon, W. S.; Iannopollo, S.; Grey, C. P.; Carlier, D.; Gorman, J.; Reed, J.; Ceder, G. *Electrochem. Solid State Lett.* **2004**, *7*, A167.
(22) Grey, C. P.; Yoon, W. S.; Reed, J.; Ceder, G. *Electrochem. Solid State Lett.* **2004**, *7*, A290.
(23) Reed, J.; Ceder, G. *Electrochem. Solid State Lett.* **2002**, *5*, A145.
(24) Yoon, W. S.; Paik, Y.; Yang, X. Q.; Balasubramanian, M.; McBreen, J.; Grey, C. P. *Electrochem. Solid State Lett.* **2002**, *5*, A263.
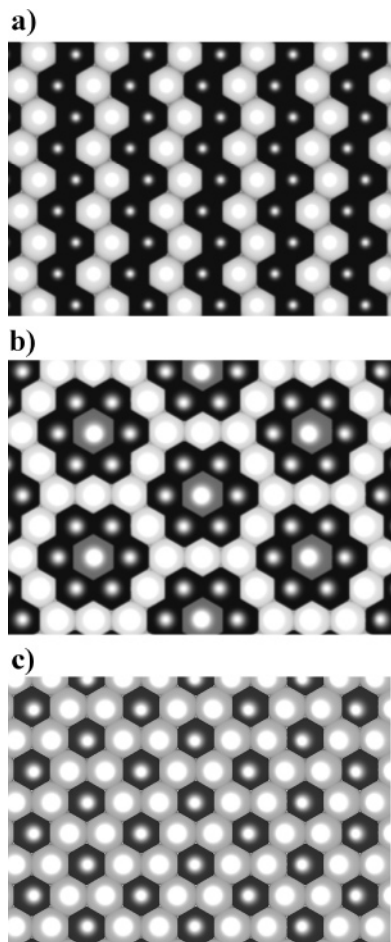
Figure 1. (a) Transition metal layer (TM layer) ordering of the zigzag structure. There is no Li in the TM layer. (b) TM layer ordering of the flower structure. There is 8.3% Li/Ni disorder, or 8.3% Li in the TM layer. Legend: black, Mn; white, Ni; gray, Li. (c) TM layer ordering of the honeycomb pattern. Legend: dark gray, α sites that can be occupied by Li or Ni; light gray, β sites that can be occupied by Ni or Mn.

to drive the ordering of Ni and Mn in the transition-metal-rich layer (TM layer) to some extent. Four different structural models of the TM layer of $LiNi_{0.5}Mn_{0.5}O_2$ have been proposed by various theoretical and experimental investigations: (1) The zigzag structure[21] in which Mn and Ni are ordered in zigzag lines without any significant amount of Li present in the TM layer (Figure 1a); 2) the flower structure with a $2\sqrt{3} \times 2\sqrt{3}$ unit cell that consists of concentric hexagons of Mn and Ni around a central Li (Figure 1b);[16] (3) the partially disordered honeycomb structure with a $\sqrt{3} \times \sqrt{3}$ unit cell[14] in which the symmetry is broken between a Mn-rich and a Li-rich sublattice (Figure 1c);[26] and (4) a disordered model without any particular ordering between Mn and Ni.[19] The honeycomb model seems to match most of the available experimental facts well. In this experimentally proposed model,[14] the TM layer is composed of two types of sites: α and β sites. The α sites are preferably occupied by either Li or Ni, and the β sites are preferably occupied by Ni or Mn. The α sites are always the nearest neighbors to a β site. The flower structure is commensurate

with the honeycomb model, but has more long-range order and can be considered as being a special case of the honeycomb model. Understanding cationic arrangement in this material is important, as the electrochemical lithiation/delithiation process and the subsequent structural stability depends on the initial structure as suggested from nuclear magnetic resonance (NMR) and first-principles studies.[16,22]

In this paper, we present computational and experimental evidence of a complex thermal disordering process: From a zigzag-like state with no Li/Ni exchange at low temperature, the system undergoes first a phase transition to a partially disordered flower structure with increasing temperature, followed by further disordering to a honeycomb superstructure at higher temperature. Our experimental verification of these computational results was made possible by the availability of samples with very little Li/Ni disorder obtained by ion exchange from $NaNi_{0.5}Mn_{0.5}O_2$.[6]

Computational Methodology

Calculations on various ordered arrangements[16,27−30] were performed in the generalized gradient approximation with Hubbard U correction to density functional theory (GGA+U). Core electron states were represented by the projector augmented-wave method[31] as implemented in the Vienna *ab initio* simulation package (VASP).[32] The PBE exchange correlation and a plane wave representation for the wavefunction with a cutoff of 370 eV were used. The Brillouin zone was sampled with a mesh including the gamma point. A $3 \times 3 \times 3$ mesh was used for the flower configuration unit cell with 48 atoms, and for cells with different sizes, a mesh with similar density was used. The charge density was spin-polarized, with Mn spins aligned ferromagnetically with other Mn and antiferromagnetically with Ni in the transition metal layer. The moment of Ni in the Li layer was aligned ferromagnetically with Mn. These spin configurations are similar to those in the flower structure.[16] The Hubbard U values in the Hamiltonian (5 eV for Mn and 5.96 eV for Ni), needed to correct for the self-interaction error on transition metals in DFT[33,34] have been calculated elsewhere[33] and are consistent with our previous work on this system.[35]

To model partially disordered states at finite temperatures, we used the cluster expansion method. This methodology is well-established for alloys[27] and has previously been used to study Li-vacancy disorder in Li_xCoO_2,[28] Li_xNiO_2,[29] and $Li_xNi_{0.5}Mn_{0.5}O_2$.[16] The cation sites are described by a lattice model, with variables describing which atom sits on each site. The essential idea is to expand the energy of the system

(25) Yoon, W. S.; Balasubramanian, M.; Yang, X. Q.; Fu, Z. G.; Fischer, D. A.; McBreen, J. *J. Electrochem. Soc.* **2004**, *151*, A246.
(26) Breger, J.; Jiang, M.; Dupre, N.; Meng, Y. S.; Shao-Horn, Y.; Ceder, G.; Grey, C. P. *J. Solid State Chem.* **2005**, *178*, 2575.

(27) Ceder, G.; Van der Ven, A.; Marianetti, C.; Morgan, D. *Modell. Simul. Mater. Sci. Eng.* **2000**, *8*, 311.
(28) Van der Ven, A.; Aydinol, M. K.; Ceder, G.; Kresse, G.; Hafner, J. *Phys. Rev. B* **1998**, *58*, 2975.
(29) de Dompablo, M.; Van der Ven, A.; Ceder, G. *Phys. Rev. B* **2002**, *66*.
(30) Zhou, F.; Maxisch, T.; Ceder, G. *Phys. Rev. B* **2006**, *97*, 155704.
(31) Blochl, P. E. *Phys. Rev. B* **1994**, *50*, 17953.
(32) Kresse, G.; Furthmuller, J. *Comput. Mater. Sci.* **1996**, *6*, 15.
(33) Zhou, F.; Cococcioni, M.; Marianetti, C. A.; Morgan, D.; Ceder, G. *Phys. Rev. B* **2004**, 70.
(34) Zhou, F.; Kang, K.; Maxisch, T.; Ceder, G.; Morgan, D. *Solid State Commun.* **2004**, *132*, 181.
(35) Breger, J.; Meng, Y. S.; Hinuma, Y.; Kumar, S.; Kang, K.; Shao-Horn, Y.; Ceder, G.; Grey, C. P. *Chem. Mater.* **2006**, *18*, 4768.

in terms of these variables. A binary−ternary coupled cluster expansion[36] was used in this work. Li and Ni were allowed to occupy sites in the Li layer (binary disorder), whereas Li, Ni, and Mn were allowed to occupy sites in the TM layer (ternary disorder). Defining the site variables as $\tau = 0$ for Li and $\tau = 1$ for Ni in the Li layer, and $\sigma = -1$ for Mn, $\sigma = 0$ for Ni, and $\sigma = 1$ for Li in the TM layer, the Hamiltonian becomes

$$E_v^{\text{predict}} = C + \sum_i V_0 \tau_i + \sum_{i,j} V^{\text{Li}}(i,j)\tau_i\tau_j + \sum_{i,j,k} \sum_{s=1}^{2} V_s^{\text{int}}$$

$$(i,j)\sigma_i^s\tau_j + \sum_{i,j,k} \sum_{s=1}^{2}\sum_{t=1}^{2} V_{st}^{\text{TM}}(i,j)\sigma_i^s\sigma_j^t + \sum_{i,j,k} V^{\text{Li}}(i,j,k)\tau_i\tau_j\tau_k +$$

$$\sum_{i,j,k} \sum_{s=1}^{2} V_s^{\text{int1}}(i,j,k)\sigma_i^s\tau_j\tau_k + \sum_{i,j,k}\sum_{s=1}^{2}\sum_{t=1}^{2} V_{st}^{\text{int2}}$$

$$(i,j,k)\,\sigma_i^s\sigma_j^t\tau_k + \sum_{i,j,k}\sum_{s=1}^{2}\sum_{t=1}^{2}\sum_{u=1}^{2} V_{stu}^{\text{TM}}(i,j,k)\sigma_i^s\sigma_j^t\sigma_k^u + \cdots \quad (1)$$

Here, V are the effective cluster interactions (ECI), and V_0 specifically acts as a site energy of the Li layer sites. The ECI V^{Li}, V^{int}, and V^{TM} represent, respectively, Li layer clusters, clusters that contain both Li and TM layer sites, and TM layer clusters. The indices i, j, and k are labels of sites in the cluster, and the dummy indices s, t, and u are used to distinguish the different ECI on the same cluster and are either 1 or 2.

Although in principle the expansion of eq 1 has to be summed over all pairs, triplets, quadruplets, and larger clusters of sites, in practice relevant cluster interactions can be selected on the basis of how well they minimize the weighted cross-validation (CV) score, which is a means of measuring how good the cluster expansion is at predicting the energy of a structure not included in the fit.[37] This amounts to neglecting the effect of configurational details beyond a certain range on the energy. The cluster expansion was fitted to the energies of 183 different configurations of Li, Ni, and Mn.

Canonical Monte Carlo (MC) simulations were conducted with this cluster expansion in cells of 2592 formula units (2592 Li layer sites, 2592 TM layer sites). In general, 50 000 equilibrium passes and 100 000 sampling passes were used at every temperature between −73 °C (200 K) and 1227 °C (1500 K). In the range near the phase transitions (477−717 °C), 100 000 equilibrium passes were used to allow better equilibration. One sampling pass amounts to one possible perturbation of each site on the lattice.

Experimental Section

LiNi$_{0.5}$Mn$_{0.5}$O$_2$ samples were prepared from ion-exchange[6] (IE-LiNi$_{0.5}$Mn$_{0.5}$O$_2$) or by conventional solid-state reaction using a coprecipitated double hydroxide[2,5,38] (SS-LiNi$_{0.5}$Mn$_{0.5}$O$_2$). As a precursor material for the IE-LiNi$_{0.5}$Mn$_{0.5}$O$_2$, layered NaNi$_{0.5}$Mn$_{0.5}$O$_2$ was prepared by solid-state reaction from a ball-milled mixture of

(36) Tepesch, P. D.; Garbulsky, G. D.; Ceder, G. *Phys. Rev. Lett.* **1995**, *74*, 2272.
(37) van de Walle, A.; Ceder, G. *J. Phase Equilib.* **2002**, *23*, 348.
(38) Lu, Z.; Dahn, J. R. *J. Electrochem. Soc.* **2001**, *148*, A237.

Table 1. Difference in Energy in meV/FU between GGA and GGA+U Approximations for Flower and Zigzag Structures

	GGA (ΔE)	GGA+U (ΔE)
flower	0 (ground state)	26
zigzag	2	0 (ground state)

Na$_2$CO$_3$ (>99.5%, Aldrich), Ni(OH)$_2$ (99.3%, J.T. Baker) and Mn$_2$O$_3$ (>99.9%, Aldrich) followed by quenching to room-temperature using copper plates. The powder was ion-exchanged with 10 times the excess amount of the eutectic composition of LiNO$_3$ (99.98%, Alfa Aesar) and LiCl (99%, Mallinckrodt) at 280 °C for 5 h in air. After ion exchange, the mixture was rinsed with distilled water and ethanol several times, filtered to recover the powder, and dried in the oven. The full ion-exchange process was repeated once more in order to complete the ion-exchange process. The SS-LiNi$_{0.5}$Mn$_{0.5}$O$_2$ was prepared by the mixed hydroxide method using LiOH·H$_2$O (98%, EM), Ni(NO$_3$)$_2$·6H$_2$O (99.999%, Aldrich), and Mn(NO$_3$)$_2$·6H$_2$O (99.99%, Aldrich). A 25 mL aqueous solution of the transition-metal nitrates was slowly dipped into 200 mL of a stirred solution of LiOH using a buret. The precipitate was filtered out, washed several times with water, and dried in the oven for a day. The dried precipitate was mixed with LiOH·H$_2$O in stoichiometric proportions and pressed into a pellet. The pellet was heated at 480 °C for 3 h in air followed by annealing at 900 °C for 12 h. The pellet was quenched to room-temperature using a copper plate.

Heat treatment of IE-LiNi$_{0.5}$Mn$_{0.5}$O$_2$ was done at 600, 800, or 1000 °C, followed by quenching in air. X-ray Diffraction (XRD) patterns were recorded from the obtained powder using a Rigaku diffractometer equipped with Cu−K$_\alpha$ radiation by step scanning (0.01°/s) in the 2θ range of 10−80°. The structural information is obtained within the $R\bar{3}m$ space group using Fullprof.[39]

Differential scanning calorimetry (DSC) measurements were conducted using a Perkin DSC7 machine. In this power-compensated calorimeter, platinum sample holders were used to avoid possible contamination of the samples. The sample is heated from room temperature to 700 °C with a heating rate of 20 °C/min.

Electron diffraction patterns and transmission electron microscope (TEM) images were collected from both the as-prepared powders and the powders after the DSC experiment. The powders were suspended on a copper grid with lacey carbon under an accelerating voltage of 200 kV on a JEOL 200CX or JEOL 2010 microscope.

Results

Comparison of GGA and GGA+U. To investigate the energy difference between structures with and without Li/Ni disorder, we calculated the energy of the flower[16] and zigzag[21] structures in the GGA and GGA+U approximations. These structures are chosen as representatives of states with (flower) or without (zigzag) Li/Ni disorder. Table 1 shows the energy differences between the two structures. Note that the energy difference in the two structures is an order of magnitude smaller in GGA than in GGA+U. This is consistent with prior work, suggesting that the flower and zigzag structures are almost degenerate in the GGA approximation.[16] As we believe the GGA+U is a more accurate description of the system (see Discussion), all energies used for the cluster expansion fit were calculated with the GGA+U approximation.

(39) Fullprof available at http://www-llb.cea.fr/fullweb/fp2k/fp2k.htm.

Table 2. Values of ECI Used in MC Calculations[a]

Pairs (meV/FU)							
Li layer pairs		interlayer pairs			TM layer pairs		
cluster	V^{Li}_{11}	cluster	V^{int}_{11}	V^{int}_{21}	cluster	V^{TM}_{11}	$V^{TM}_{21} = V^{TM}_{12}$	V^{TM}_{22}
2	107.5	5	−90.8	22.2	9	434.8	73.0	656.7
3	−6.1	6	−101.8	52.4	10	−24.6	7.2	1.2
4	−32.3	7	18.7	11.0	11	15.5	14.2	31.0
		8	−13.1	−1.2	12	71.3	−15.1	8.7

Triplets (meV/FU)						
Li−Li−TM triplets			TM−TM−TM triplets			
cluster	V^{int1}_1	V^{int1}_2	cluster	V^{TM}_{111}	$V^{TM}_{112} = V^{TM}_{121} = V^{TM}_{211}$	$V^{TM}_{122} = V^{TM}_{212} = V^{TM}_{221}$	V^{TM}_{222}
13	17.8	−21.5	15	−25.0	25.8	−13.1	−61.3
14	30.8	−90.1	16	113.7	12.3	−45.1	−378.7

[a] Point cluster: $V_0 = -452.6$ meV/FU. Clusters corresponding to each number are shown in Figure 8.
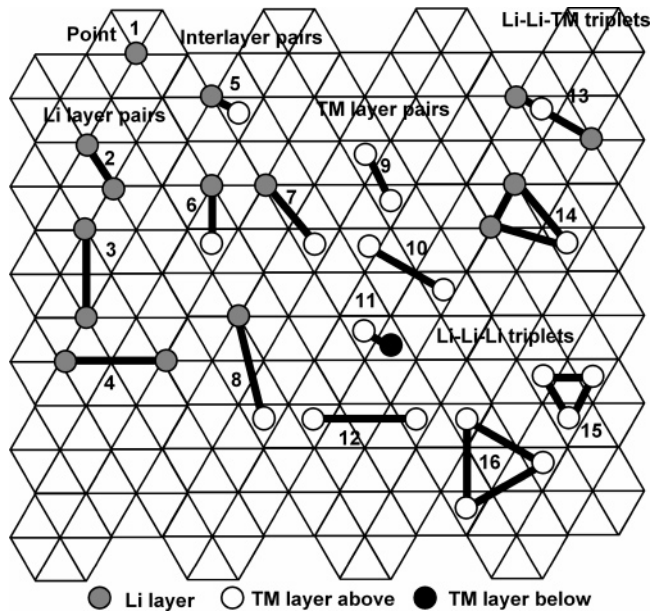
Figure 2. Clusters used in the cluster expansion.

Cluster Expansion. In our cluster expansion, clusters were selected from a pool including all pair interactions up to seventh cation−cation nearest-neighbor (NN) distance and triplets that contain pair clusters up to the third-NN distance as subclusters. Pairs that span over three or more cation layers and triplets that include only sites in the Li layer were removed. There are 1 empty cluster, 1 point cluster, 22 pair clusters, and 28 triplet clusters in the pool. From this pool, a set of relevant clusters and ECI were obtained, with a weighted average CV score of 6.94 meV/FU and weighted root-mean-square error of 3.43 meV/FU. One formula unit (FU) consists of one lithium ion, one transition-metal ion, and two oxygen ions. The CV score may be thought as the prediction error. Because the energy difference between flower and zigzag structures is 26 meV/FU (see Table 1), a CV score of about 7 meV can be considered to be small enough for this study. Table 2 shows the ECI obtained from this fit, and the clusters defining the interactions are shown in Figure 2. Note that clusters including sites that can be occupied by three species (TM layer sites) need multiple ECI per cluster to independently represent the energy contribution of each possible configuration on that cluster. For a more detailed discussions of ternary and higher component rep-

resentations in the cluster expansion, we refer the reader to references 40−42.

In the MC calculations, the set of ECI in Table 2 is used. However, an additional penalty of 1 eV per pair is added to Ni−Ni pairs in the Li layer to avoid Li/Ni segregation in the Li layer, because it is well-known experimentally that there are no clusters of Ni in the Li layer. This penalty needed to be added because it was not possible to accurately sample first-principles energies of structures that include NN Ni− Ni pairs in the Li layer, as spin density integration revealed that electrons did not localize properly on Ni for these calculations because of their strong electrostatic repulsion. This is an indication that such configurations are very high in energy. The exact magnitude of the penalty is not important. As long as these configurations do not appear in the simulation, they do not affect the value of the average energy.

MC Simulation. Figure 3a shows the thermally averaged energy as a function of increasing temperature in MC calculations starting from either a zigzag structure or a flower structure. Even though the flower structure has higher energy at low temperature, it does not transform to the zigzag configuration, indicating that the flower configuration is metastable. However, the energy at low temperatures in a MC calculation starting from the partially disordered flower structure (about 10 meV/FU) is significantly lower than the ground-state energy of the perfect flower structure (about 26 meV/FU). This indicates that some change occurs in the structure with essentially no kinetic barrier; the driving force of such change will be further discussed later. The zigzag structure undergoes a phase transition close to $T_1 \approx 550$ °C. Above this temperature T_1, the energies in MC simulations starting from flower and zigzag become the same, indicating that the two initial phases end up in the same phase. An additional phase transition occurs at $T_2 \approx 620$ °C in both sets of calculations.

Figure 3b shows the thermally averaged heat capacity of the calculations. This heat capacity includes only the effect

(40) McCormack, R.; de Fontaine, D.; Wolverton, C.; Ceder, G. *Phys. Rev. B* **1995** *51*, 15808.
(41) Ceder, G.; Garbulsky, G. D.; Avis, D.; Fukuda, K. *Phys. Rev. B* **1994**, *49*, 1.
(42) Inden, G.; Pitsch, W. *Materials Science and Technology: A Comprehensive Treatment*; Cahn, R. W., Haasen, P., Kraamer, E. J., Eds.; John Wiley & Sons: New York, 1991; p 497.
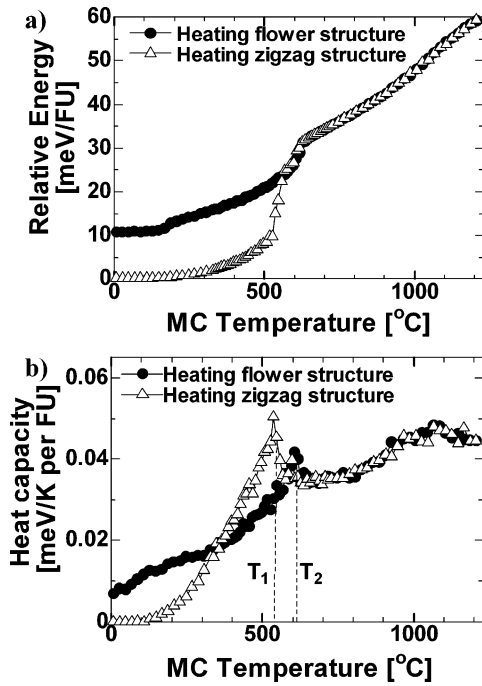
Figure 3. (a) Monte Carlo energy as a function of temperature. (b) Monte Carlo heat capacity as a function of temperature.
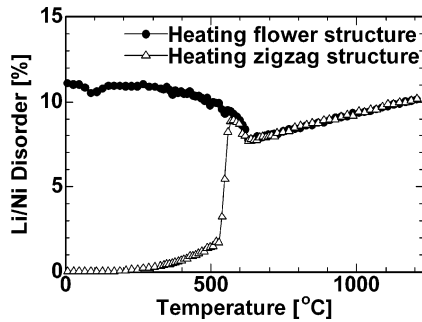

Figure 4. Calculated Li/Ni exchange between the Li and TM layers as a function of temperature.

Figure 5. Monte Carlo snap shot of (a) transition-metal-rich layer; (b) Li-rich layer at $T = 577$ °C (850 K). Legend: black, Mn; white, Ni; gray, Li.

of configurational entropy. The simulation that starts from the zigzag structure shows two heat-capacity peaks at T_1 and T_2, consistent with the two phase transitions observed in the energy in Figure 3a. The heat capacity peak in the simulation starting from the flower structure shows only a single peak at T_2.

Figure 4 shows the Li/Ni disorder, measured as the concentration of Ni in the Li layer averaged over 50 snapshots of structures at each temperature. The snapshots of the structures were taken at regular intervals (every 2000 passes) during the sampling calculations. The Li/Ni disorder of the zigzag phase is close to zero at the start of the simulation; however, it increases to 8−9% at the first phase transition at $T = T_1$. Above $T > T_1$, the Li/Ni disorder amount seems to be independent of the starting configuration of the simulation, consistent with the results of the energy and heat capacity calculations.

Figure 5 shows a snapshot of the structure at 577 °C (850 K), which is just above the first phase transition. Figure 5a from the MC simulation is a good representation of the cation arrangement in the TM layer at this temperature range regardless of the starting configuration. There are well-formed "flower" rings consisting of a Li ion surrounded by
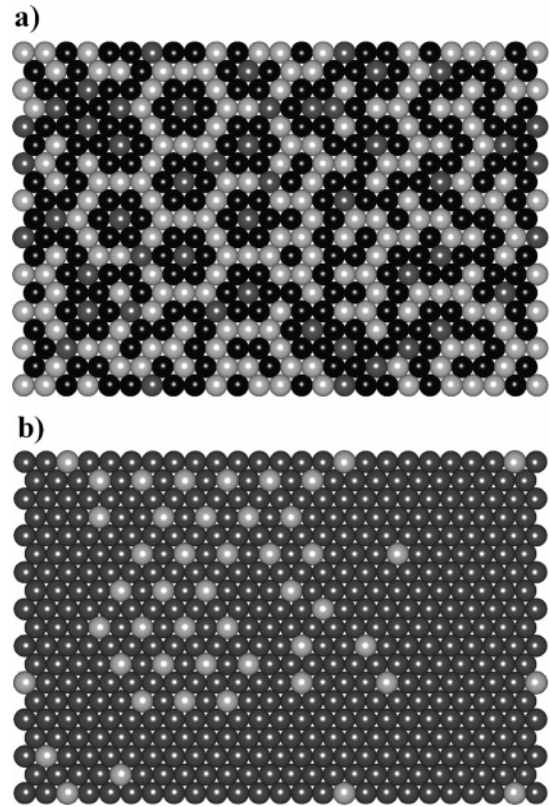
six Mn ions, which in turn are surrounded by a larger Ni ring. However, substantial disorder, such as LiMn$_5$Ni rings, Ni−Mn zigzag domains, and even a few MnNi$_6$ rings, are present. The presence of Li surrounded by five Mn and one Ni (as in a LiMn$_5$Ni ring) was observed in NMR spectra.[21] The ordering in the TM layer seems to correlate clearly with the ionic occupation and ordering in the adjacent Li layers. This point will be discussed further below.

The cation ordering patterns in the MC simulations show significant local charge imbalance in structures below T_2. When flower patterns exist, as shown in Figure 5a, there is a corresponding 2×2 ordering pattern of Ni and Li, as seen in Figure 5b, making this specific area excess in Ni. The MC snapshot of the specific Li layer in Figure 5b has a concentration of Ni that is a few percent higher than the average Li/Ni disorder value in Figure 4, although the MC cell as a whole is charge-balanced.

As can be observed in a snapshot of the structure at 927 °C (1200 K; Figure 6), the Ni present in the Li layer disorders above T_2 and no longer arranges in 2×2 patterns. Although the TM layer shown in Figure 6a apparently looks completely disordered, the average site occupations correspond to the honeycomb scheme mentioned before.[21,22] Li and Ni positions seem to be uncorrelated in the Li layer, as shown in Figure 6b.

XRD. Figure 7 shows the XRD patterns of LiNi$_{0.5}$Mn$_{0.5}$O$_2$ obtained through ion-exchange from layered NaNi$_{0.5}$Mn$_{0.5}$O$_2$ (IE-LiNi$_{0.5}$Mn$_{0.5}$O$_2$) and through solid-state reaction (SS-LiNi$_{0.5}$Mn$_{0.5}$O$_2$).[6] The IE-LiNi$_{0.5}$Mn$_{0.5}$O$_2$ has a larger I_{003}/I_{104} ratio (1.74 for IE-LiNi$_{0.5}$Mn$_{0.5}$O$_2$ versus 1.26 for SS-LiNi$_{0.5}$Mn$_{0.5}$O$_2$) and well-defined splitting of (006)/(012) and (018)/

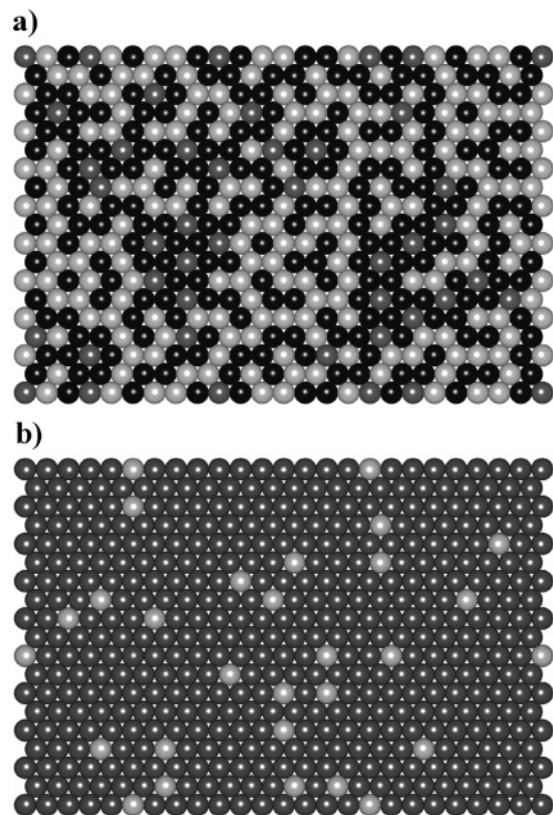**Figure 6.** Monte Carlo snap shot of (a) transition-metal-rich layer; (b) Li-rich layer at $T = 927$ °C (1200 K). Legend: black, Mn; white, Ni; gray, Li.
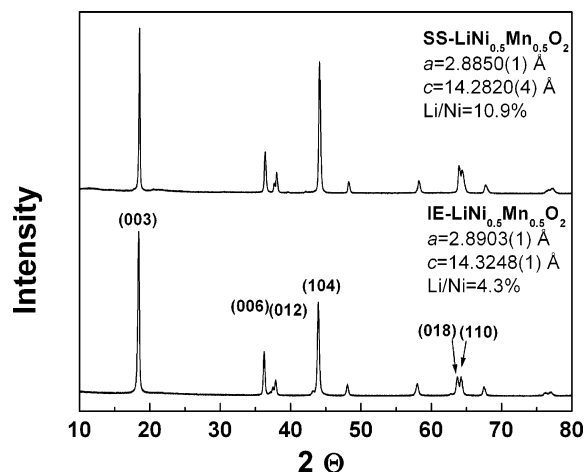

Figure 7. Comparison of the XRD spectra of SS$-$LiNi$_{0.5}$Mn$_{0.5}$O$_2$ and IE-LiNi$_{0.5}$Mn$_{0.5}$O$_2$.

(110) peaks in Figure 7, which is believed to be an indication of a more layered structure.[2] The Rietveld refinement of each profile gives lattice parameters that are in good agreement with previous reports on those materials.[2,14,15,19−22,43] Trace amounts of NiO were detected in IE-LiNi$_{0.5}$Mn$_{0.5}$O$_2$. Flower ordering is driven by the presence of Li in the TM layer, as it was previously shown that the ground-state ordering when Li/Ni disorder is prevented is the zigzag structure.[21] Hence, we expect IE-LiNi$_{0.5}$Mn$_{0.5}$O$_2$ with little or no Li/Ni disorder to be a system representative of what occurs to the zigzag ordering in our MC simulation. Because SS-LiNi$_{0.5}$Mn$_{0.5}$O$_2$ has an amount of Li/Ni disorder comparable to the flower
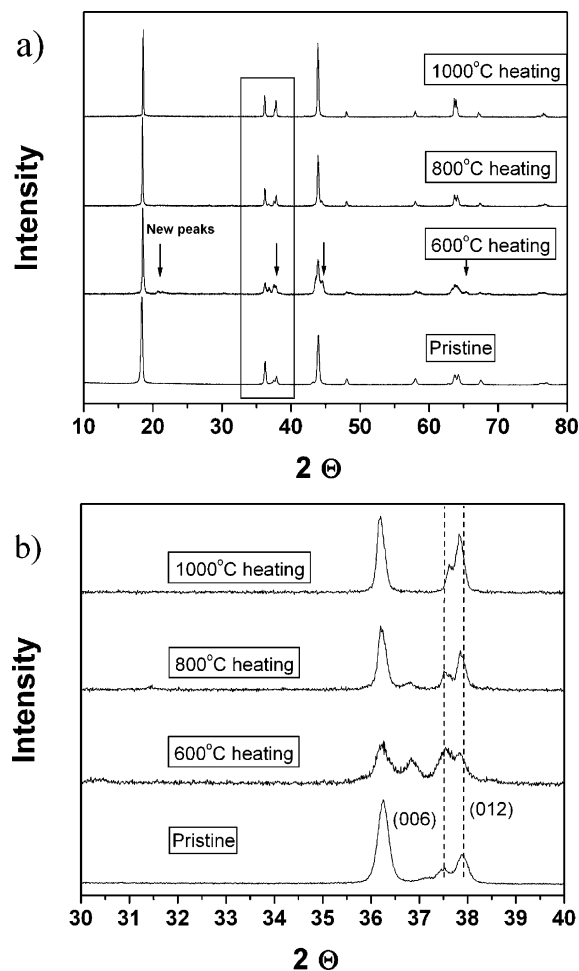
(43) Reed, J.; Ceder, G. *Electrochem. Solid State Lett.* **2002**, *5*, A145.

Figure 8. (a) XRD spectra of IE-LiNi$_{0.5}$Mn$_{0.5}$O$_2$ after heating at different temperatures. (b) Enlargement of area around the (006) and (012) peaks.

structure, it will be compared to the result of MC calculations starting from the flower configuration.

Figure 8 shows the XRD profiles of IE-LiNi$_{0.5}$Mn$_{0.5}$O$_2$ after annealing at 600, 800, and 1000 °C. It appears that major structural change has already started to occur at 600 °C, where the broadening of peaks and evolution of new peaks are observed. We could not identify the new peaks, but because they appear only near the existing peaks from the layered structure, we suspect that they are from structures that are closely related to the original layered one. The new peaks around 21−22° are similar to the ones observed when Li−Mn$_6$ rings are present in the TM layer of a layered structure.[26] At 800 and 1000 °C, well-defined sets of peaks re-appear at the expense of the new peaks that arose at 600 °C. Trace amount of these new peaks that occurred at 600 °C still exist at 800 °C. The evolution of the (006)/(012) peaks, enlarged in Figure 8b, and the (018)/(110) peaks clearly shows that the layered characteristics reduce as the heating temperature increases. Rietveld refinement of the profiles was attempted within the $R\bar{3}m$ space group, except for the sample heated at 600 °C, for which peaks are not well-defined. Table 3 shows the refined lattice parameters and the amount of Li/Ni disorder for each sample. The amount of Li/Ni disorder increases as the heating temperature increases, as expected. Also, the c/a ratio decreases with temperature. This is fully consistent with the results from heating the zigzag ordered structure in our MC simulation.

Table 3. Rietveld Refinement Results on Li/Ni Disorder as a Function of Temperature

T (°C)	Li/Ni disorder (%)	a (Å)	c (Å)	c/a	R_b	R_{exp}
pristine	4.3	2.8903(1)	14.3248(1)	4.956	7.83	10.0
800	11.2	2.9009(1)	14.3406(1)	4.944	16.2	18.5
1000	14.7	2.9123(1)	14.3519(1)	4.928	15.1	7.74

The annealing of IE-LiNi$_{0.5}$Mn$_{0.5}$O$_2$ at 1000 °C shows a relatively high Li/Ni disorder of 14.7% and large *a* and *c* lattice parameters. The reason for this is not clear yet, but it can be related to a formation of a spinel-like phase, which will be further explained in the discussion section. Due to the nature of the ion-exchange process, a small amount of Li deficiency in the material may be present. Layered structures with Li deficiency are known to be susceptible to phase transformation to spinel.[8] Nevertheless, observable peak splittings of (006)/(012) and (018)/(110) in the XRD pattern of 1000 °C (Figure 8a) indicate that the majority of the structure remains in a layered form.

DSC. Figure 9 shows the DSC data of two distinct samples: IE-LiNi$_{0.5}$Mn$_{0.5}$O$_2$ and SS-LiNi$_{0.5}$Mn$_{0.5}$O$_2$. The amounts of the two samples are similar, weighing approximately 10 mg each. An endothermic peak is clearly seen in IE-LiNi$_{0.5}$Mn$_{0.5}$O$_2$ upon heating, indicating an equilibrium first-order phase transition around 600 °C. The DSC curve of SS-LiNi$_{0.5}$Mn$_{0.5}$O$_2$ is relatively flat, showing no significant structural change in the compound upon heating.

TEM. Figure 10a and 10b shows TEM images of IE-LiNi$_{0.5}$Mn$_{0.5}$O$_2$ before and after the DSC experiment in which the sample was heated to 700 °C. A representative electron diffraction pattern from zone axis $[\bar{1}1\bar{1}]_{hex}$ of the IE-LiNi$_{0.5}$Mn$_{0.5}$O$_2$ (Figure 10c) shows no superstructure intensities. It indicates that the $\sqrt{3} \times \sqrt{3}\ a_{hex}$ superstructure, often observed in SS-LiNi$_{0.5}$Mn$_{0.5}$O$_2$, is not present in IE-LiNi$_{0.5}$Mn$_{0.5}$O$_2$. This provides additional evidence that IE-LiNi$_{0.5}$Mn$_{0.5}$O$_2$ has more characteristics of a layered structure with less Li/Ni disorder. The fundamental reflections and the zone axes are indexed to the parent hexagonal cell with rhombohedral symmetry and space group $R\bar{3}m$. Figure 10d shows the $[\bar{1}1\bar{1}]_{hex}$ zone axis pattern collected from the IE-LiNi$_{0.5}$Mn$_{0.5}$O$_2$ sample after the DSC experiment. The two most predominant features are the sextet of the (110) type reflection and the doubling of the ($\bar{1}$12) type reflection in the electron diffraction image, which suggest the formation of a $2\sqrt{3} \times 2\sqrt{3}\ a_{hex}$ superstructure. The superstructure is consistent with the flower structure. The insert next to the highlighted area in Figure 10d is the simulated ED pattern from the flower superstructure. The absence of certain superstructure reflections in Figure 10d is suspected to be due to minor stacking disorder of the ordered planes along c_{hex}. The bright-field (Figure 11a) and dark-field (Figure 11b) images of IE-LiNi$_{0.5}$Mn$_{0.5}$O$_2$ after the phase transition clearly show the phase boundaries between transformed and untransformed material. The coexistence of two phases after DSC run to 700 °C is consistent with the XRD results of the samples annealed at 600 and 800 °C, which show shoulders next to the (104) peak.
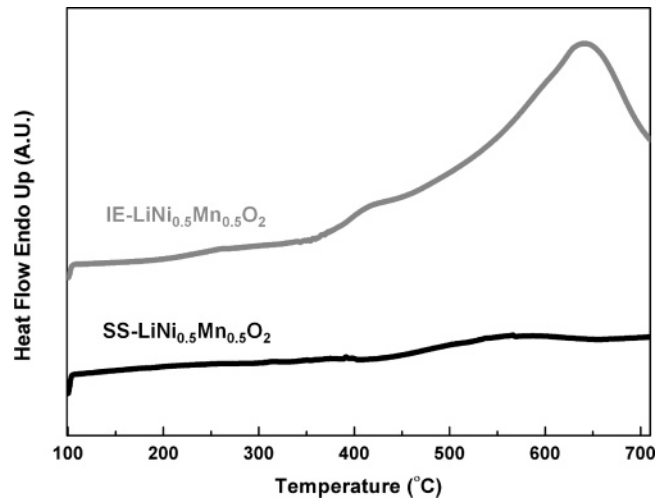
Figure 9. DSC results of IE-LiNi$_{0.5}$Mn$_{0.5}$O$_2$ and SS-LiNi$_{0.5}$Mn$_{0.5}$O$_2$.

Discussion

Magnetic Interactions in GGA vs GGA+U. Our computational results indicate a significant difference between the GGA and GGA+U approximations for the ground state of LiNi$_{0.5}$Mn$_{0.5}$O$_2$ (Table 1). Whereas in GGA the flower and zigzag structures are nearly degenerate, the zigzag structure is clearly the ground state in GGA+U. This is at first somewhat surprising. We have previously demonstrated that the use of GGA+U is critical to obtaining the ground state and phase diagram of mixed-valence systems,[30,33] but LiNi$_{0.5}$Mn$_{0.5}$O$_2$ has no mixed-valence transition-metal ions and Ni and Mn are clearly +2 and +4 in GGA.[43]

We believe that the difference in energies of the zigzag and flower structures in the GGA and GGA+U approximations can be attributed to the difference in electron localization[34] in both methods, which in turn affects the magnetic interactions. In GGA, excessive delocalization of the transition metal 3*d* states onto oxygen leads to the overestimation of superexchange effects. Because the particular ordering of the Ni and Mn ions in the flower structure benefits from the antiferromagnetic coupling between the Ni in the Li layer and the Ni in the TM layer, the flower structure is more favored in the GGA approximation.[16]

GGA+U reduces the hybridization between the transition metals and oxygen thereby decreases the superexchange coupling. This effect shows up as a different magnetic ground state in the flower structure in GGA and GGA+U.[44] In both theories, the Ni spin in the TM layer is antiferromagnetically aligned to the Ni spin in the Li layer. Nevertheless, wheras in GGA the Ni and Mn spins in the same TM layer are antiferromagnetically aligned, and all Mn spins are aligned ferromagnetically, in GGA+U, Mn spin of adjacent TM layers are aligned antiferomagnetically, implying that in half of the TM layers, Ni and Mn spins are antiferromagnetically aligned, but ferromagnetically aligned in the other half of TM layers. The predicted magnetic remanence of the flower structure is 0.99 μ_B/FU in GGA and 0.24 μ_B/FU in GGA+U

(44) Hinuma, Y.; Meng, Y. S.; Kang, K.; Ceder, G. *Computational Investigation of LiNi$_{1/2}$Mn$_{1/2}$O$_2$*, Presented at the Materials Research Society Fall 2005 Meeting, Boston, MA, Nove 27−Dec 1, 2005; Materials Research Society: Warrendale, PA, 2005.
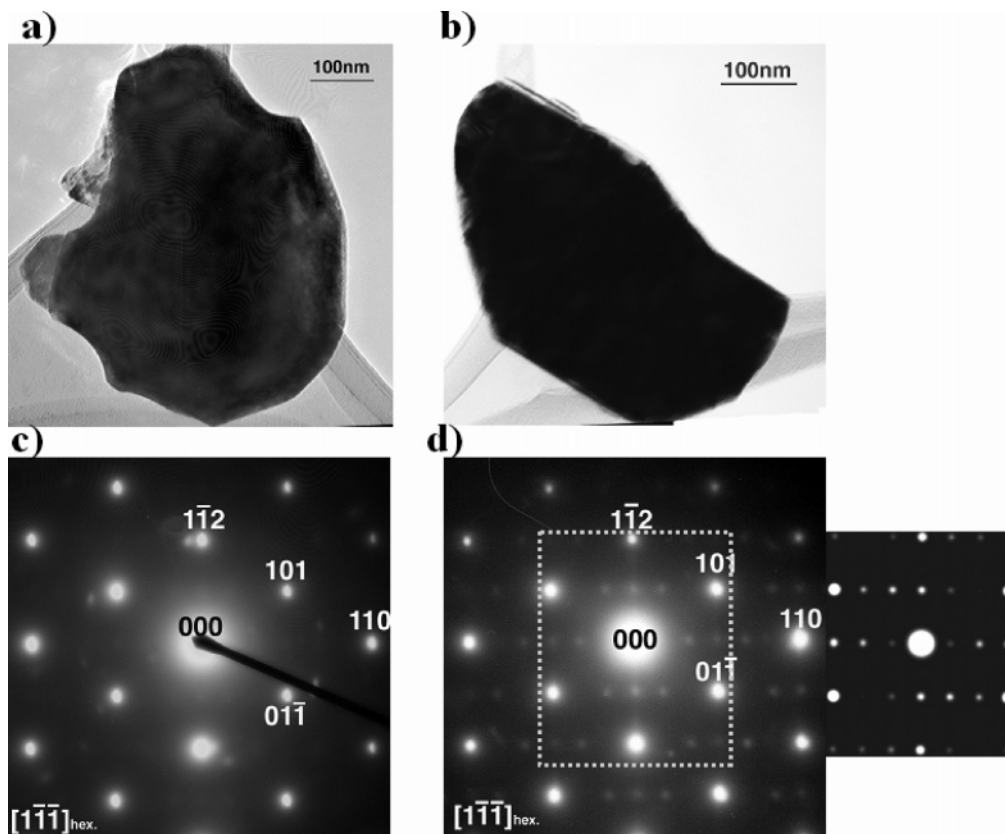
Figure 10. TEM images of IE-LiNi$_{0.5}$Mn$_{0.5}$O$_2$ (a) before and (b) after phase transition, and (c, d) corresponding electron diffraction patterns. The insert next to part d is a simulated electron diffraction pattern of the flower structure with one particular stacking. The simulation is done with CrystalMaker.
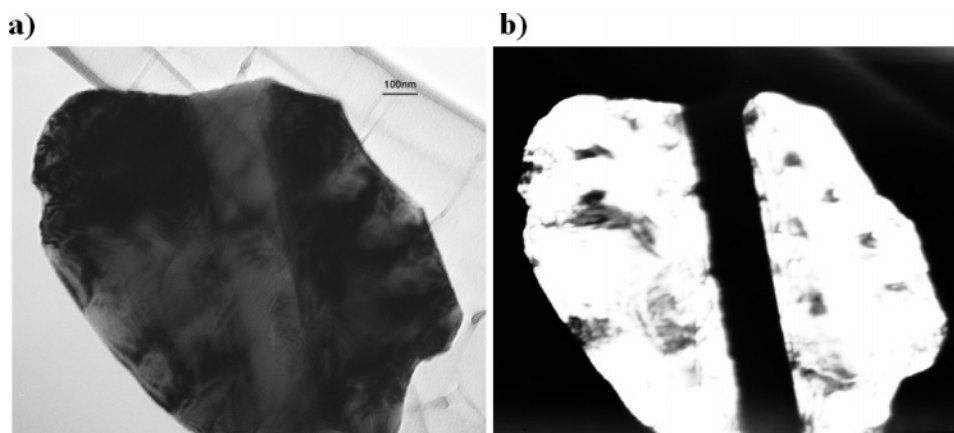

Figure 11. TEM image after heating to 700 °C shows the IE-LiNi$_{0.5}$Mn$_{0.5}$O$_2$ in the midst of a first-order phase transition: (a) bright-field and (b) dark-field.

(effective magnetic moment for Ni^{2+} is 2.82μ_B and 3.87μ_B for Mn^{4+}). The experimentally observed remanence of SS−LiNi$_{0.5}$Mn$_{0.5}$O$_2$, which is likely to be close to the partially disordered flower structure, is 0.17−0.20 μ_B/FU.[44] Hence, GGA+U may be a more proper description of the structural energetics than GGA, especially when magnetic interactions greatly affect the relative stability between structures. It may also be noted that in the similar Li$_2$MnO$_3$ system, Mn^{4+} ions in different TM layers interact antiferromagnetically.[45] Because of the better agreement with experimental data on magnetism, we have used the energies from the GGA+U approximation in the cluster expansion in this paper. The spin magnetic configuration in reference[16] was used in the cluster expansion of GGA+U energies.

(45) Strobel, P.; Lambertandron, B. *J. Solid State Chem.* **1988**, *75*, 90.

Driving Force for the Order−Disorder Transformation in the Flower Structure. The MC simulation shows the energetically stable cation ordering in the LiNi$_{0.5}$Mn$_{0.5}$O$_2$ system as a function of temperature and reveals some of the physics that drives the ordering. The flower structure can be considered to be a superstructure of the honeycomb structure. In the flower ordering, Li orders in $2\sqrt{3} \times 2\sqrt{3}$ patterns in the TM layer. This pattern can be mapped perfectly onto the α sites of the honeycomb pattern, which has $\sqrt{3} \times \sqrt{3}$ ordering. The central Li atoms in the flower structure occupy 1/4 of the α sites, with Ni occupying the other α sites. Mn ions that occupy the six sites surrounding Li are all located on β sites. Hence the transformation from the partially ordered flower structure to honeycomb ordering is an order−order transformation whereby Li and Ni disorder

on the α sites. Several physical interactions seem to contribute to the ordering into a flowerlike arrangement. Flower ordering was previously shown[46] to be the electrostatically favored configuration of +1, +2, and +4 cations on a two-dimensional triangular lattice describing the TM layer. However, this by itself does not seem to fully capture the energetics of the flower structure. The difference between the GGA and GGA+U results points at the Ni$_{TM}$−O−Ni$_{Li}$ superexchange between Li and TM layers as driving the honeycomb ordering to further order into the flower arrangement.[16] When the spins on the Ni in the TM layer and Li layer are aligned antiferromagnetically, the Ni 3d orbitals can each hybridize with the same spatial (but different spin) oxygen 2p orbital and delocalize onto the oxygen. This interaction is consistent with the Goodenough−Kanamori rules.[47] We have some evidence that this antiferromagnetic interaction is crucial for the stability of the flower. When Ni spins are forced to be ferromagnetic in GGA calculations, the flower structure is not the most stable state.[16] Furthermore, flower patterns do not form without Li in the TM layer, or in other words, without including Ni in the Li layer.[21] A similar case in which interactions that bridge an oxygen are an important factor in the structural stability is the Li$_A$−O−Ni^{3+}−O−Li$_B$ 180° interaction in LiNiO$_2$.[48,49]

As seen in Figure 5, the flower pattern in the MC simulations is accompanied by a 2 × 2 ordering of Ni in the Li layer. The stability of the 2 × 2 pattern can be rationalized by looking at the flower structure in three dimensions (Figure 12a). The top and bottom layers show the flower patterns in the TM layer. There are three sites for each flower unit in the Li layer between the two layers (shown in dark gray) that can have the maximum, or four, Ni$_{TM}$−O− Ni$_{Li}$ bonds. Occupation of all these sites by Ni results in 2 × 2 ordering of Ni in the Li layer, as is observed in the MC calculations.

The competition between the Ni$_{TM}$−O− Ni$_{Li}$ bonding and local charge neutrality leads to frustration in the flower-ordered LiNi$_{0.5}$Mn$_{0.5}$O$_2$ system. Complete 2 × 2 ordering of Ni in the Li layer would lead to a local charge imbalance in regions that are perfectly flower-ordered in the TM layer. The solution to these competitive forces seems to be to create somewhat higher Li/Ni disorder than the 8.33% (1/12) of the perfectly ordered flower structure. This additional Li/Ni exchange creates more (less) Ni in the Li (TM) layer and as such increases the number of Ni$_{TM}$−O−Ni$_{Li}$ bonds that can be formed. This is why more Li/Ni disorder is created (about 11%) in the MC simulations as soon as the temperature is above 0 K (Figure 4). However, increasing Li/Ni exchange leads to more Li in the TM layer flower sites other than the core site of the flower. The Li in sites other than the core site has higher site energy, as it is coordinated by only three or four Mn. Therefore, a Li/Ni exchange of 8−11% is observed as a balance of creating favorable Ni$_{TM}$−O− Ni$_{Li}$ bonds and unfavorable Li sites in the TM layer. This may

(46) Ceder, G.; Meng, Y. S.; Gorman, J. P.; Hinuma, Y.; Shao-Horn, Y.; Grey, C. P. *Ordering in Li[Ni$_x$Li$_{1/3-2x/3}$Mn$_{2/3-x/3}$]O$_2$ Systems: Theory and Experiment* 12th International Meeting on Lithium Batteries, Nara, Japan, June 27−July 2, 2004; Electrochemical Society: Pennington, NJ, 2004.
(47) Kanamori, J. *J. Phys. Chem. Solids* **1959**, *10*, 87.
(48) de Dompablo, M.; Ceder, G. *Chem. Mater.* **2003**, *15*, 63.
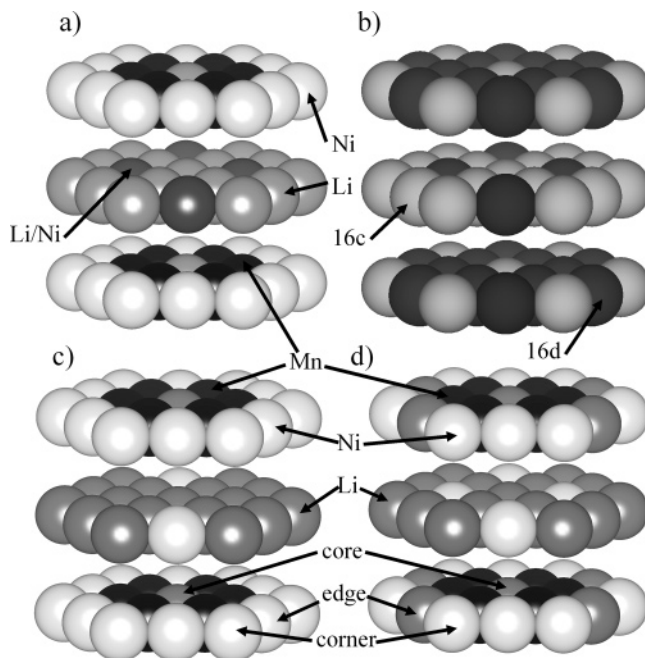(49) de Dompablo, M.; Ceder, G. *J. Power Sources* **2003**, *119*, 654.

Figure 12. (a) Flower structure with emphasis on the interaction across layers. Of the 12 sites in the Li layer per flower unit, there are three sites that have four Ni−Ni second-nearest neighbors. The Ni in the Li layer prefers these sites. Legend: black, Mn; white, Ni; light gray, Li; dark gray, Li/Ni sites. (b) The flower unit viewed in the spinel setting. Legend: light gray, Li-rich 16c sites; dark gray, Li-poor 16d sites. (c) Perfect flower structure. (d) Partially disordered flower structure with lower first-principles energy than the flower shown in part c. Legend: black, Mn; white, Ni; gray, Li.

also explain why the Li/Ni disorder decreases with temperature: As the flower structure partially disorders, the frustration between the local charge balance and the Ni$_{TM}$−O−Ni$_{Li}$ bonding can be more easily resolved and requires less additional Li/Ni exchange. Note in particular how the Li/Ni disorder rapidly decreases in our simulation as the partially disordered flower further disorders into the honeycomb structure at about 620 °C (see Figure 4).

Partially Disordered Flower Structure. One way to understand the partially disordered flower structure is to look at the structure in both the layered $R\bar{3}m$ and the spinel $Fd\bar{3}m$ space group settings. In LT-LiCoO$_2$, an example of a lithiated spinel-like material, Li occupies 16c sites and Co occupies 16d sites.[4] The relations between the flower structure in the layered and spinel space group settings are similar and depicted in Figure 12. Figure 12b shows the layered flower structure, but with the sites marked in the spinel setting: the Li layer is composed of 75% 16c sites and 25% 16d sites, and the TM layer is composed of 25% 16c sites and 75% 16d sites. The possible Ni sites in the Li layer that create more Ni$_{TM}$−O−Ni$_{Li}$ superexchange bonds are labeled as Li/Ni sites in Figure 12a. Note that these Li/Ni sites correspond to the Li layer 16d sites in Figure 12b. The 16c sites in the Li layer are unlikely to contain Ni, because these sites do not have the maximum possible Ni$_{TM}$−O−Ni$_{Li}$ superexchange bonds when the TM layer has a perfect flower ordering. The 16c sites in the TM layer (top and bottom layers of Figure 12b) correspond to the "core" of the flower (the site surrounded by a Mn ring) and the six "corners" of the flower. Each corner is simultaneously a corner of three flower motifs, so there are two corner sites for each core

site. The core is Li and the corners are Ni in the perfect flower structure in Figure 12c. This means that out of the 16*c* sites in the TM layer, which amount to 25% of all 16c sites, about 2/3 of them are occupied by Ni. As there is no Ni in the 16*c* sites of the Li layer, in the flower model Ni occupies 1/6 (16.7%) of the total 16c sites in the spinel setting. On the other hand, Li occupies 2/3 of the 16*d* sites in the Li layer in the flower structure. In fact, full occupation of all 16*d* sites in the Li layer by Ni can happen with relatively low energy penalty if the additional Li created in the TM layer occupies only the 16*d* sites in the TM layer ("edge" sites). This exchange leads to the extreme case of a partially disordered flower structure as shown in Figure 12d: an ordered structure with all Li/Ni sites (16*d*) in the Li layer occupied by Ni. In the TM layer, Li occupies some flower "edge" sites (16*d*), maintaining charge balance of the system as a whole. This configuration has lower energy than the perfect flower structure in GGA+U calculations, but still higher than the zigzag structure because of unfavorable Li site occupation in the TM layer. Interestingly, the Li occupancy on the TM-rich 16*d* sites or the Ni occupancy on the Li-rich 16*c* sites is 1/6, although in this scenario, the Li/Ni disorder has increased from 8.33 to 25%. It can be clearly seen that the partially disordered flower structure has the characteristics of both layered (with 3*a*/3*b* disorder) and spinel (with 16*c*/16*d* disorder) features. One example of such a case is in the LiNi$_{0.5}$Mn$_{0.5}$O$_2$ sample annealed at 600 °C by Lu et al.[4] Rietveld refinement showed 16.1% Li/Ni disorder between the Li and TM layers in the layered setting and 17.4% Li/Ni disorder between Li-rich 16c sites and TM-rich 16d sites in the spinel setting.[4]

Phase Transitions. As seen in Figures 3a, 3b, and 4, the MC simulation clearly shows that upon heating of the zigzag structure, at a certain critical temperature T_1, a phase transition occurs to the flower phase. Because the perfect flower structure has higher energy at 0 K, it must have achieved higher entropy than the zigzag structure at T_1. The entropy difference can be rationalized through the excitations available for both phases. The zigzag phase has fewer low-energy excitation states compared to the flower phase. The excitations observed in snapshots of the MC simulation from the zigzag phase are simple exchanges of Li and Ni between Li and TM layers. But Li in the TM layer prefers to be surrounded by all Mn, which is not possible when it occupies a Ni position in the zigzag structure. Breaking the zigzag ordering in the TM layer requires relocation of a large number of cations, which is difficult in MC simulations at low temperatures. Therefore, putting Li in the TM layer of the zigzag phase carries a heavy energy penalty, because Li can at best be surrounded by four Mn. In contrast, in the flower phase, the majority of Li are surrounded by six Mn. In addition, in the TM layer the flower patterns can form and disintegrate relatively easily in the honeycomb framework.[21,22] The honeycomb ordering guarantees that no Li−Li nearest-neighbor pairs occur in the TM layer, which would come with a strong electrostatic energy penalty. Because of the difference in excitations, the flower phase becomes stable above a certain temperature where the zigzag phase cannot tolerate much Li/Ni disorder.

Such a phase transition from a low Li/Ni disorder phase to a high disorder phase is indeed observed experimentally using both XRD and DSC/TEM, and together with the simulation results paint a consistent picture of the phase evolution of LiNi$_{0.5}$Mn$_{0.5}$O$_2$. According to the simulation results, IE-LiNi$_{0.5}$Mn$_{0.5}$O$_2$, representative of a material with little or no Li/Ni site disorder, is probably the stable phase at low temperature and transforms to a partially disordered flower arrangement near 550 °C. The phasetransition temperature as observed by DSC measurement is about 600 °C. In DSC, the latent enthalpy obtained from peak integration of the phase transition of IE-LiNi$_{0.5}$Mn$_{0.5}$O$_2$ is about 1.2 kJ/mol, but could not be accurately determined because the phase transition is unfinished at 600 °C (some large particles are only partially transformed, as shown in Figure 11). In the MC simulation, the latent heat for this transformation is about 1 kJ/mol, consistent with the DSC result.

We also found in our MC simulations that the phase transition from zigzag to flower is not reversible upon cooling. Upon cooling, the values of the energy, heat capacity, and Li/Ni disorder closely track the values upon heating the flower structure. Because zigzag is the thermodynamic ground state at low enough temperature, this can be explained only by a kinetic limitation. One possible reason for the irreversibility may lie in the extreme stability of the Li in the transition-metal layer. Those Li ions are typically surrounded by five or six Mn ions, and this configuration is very difficult to break up because of its favorable short-range electrostatic interactions. This keeps the Li ions in the transition-metal layer and prevents the formation of zigzag configurations. Such kinetic limitations observed in our first-principles MC simulations may be a representation of reality, because even slow cooling of LiNi$_{0.5}$Mn$_{0.5}$O$_2$ samples from above T[1] never leads to low Li/Ni disorder.

In the MC simulation, upon heating above temperature T_2 (∼620 °C) the partially disordered flower structure undergoes a phase transition to the honeycomb structure. The well-defined heat capacity peak in Figure 3b indicates that this is a phase transition, rather than a gradual disordering of the flower structure. We were not able to study this transition in our DSC experiment because of the limited temperature range and resolution of the instrument. However, this phase transition implies the existence of a possible intermediate phase between the ground state and the high-temperature disordered state of LiNi$_{0.5}$Mn$_{0.5}$O$_2$, and may be a reason why some of the literature shows that the electrochemical behavior of LiNi$_{0.5}$Mn$_{0.5}$O$_2$ strongly depends on the processing temperature.[4,19]

The combined simulation and DSC data lead us to propose the phase diagram in Figure 13. The temperatures included are derived from the simulations. At low temperature, a structure with little or no Li/Ni exchange is the ground state. Above ∼550 °C, this structure transforms to a partially disordered flower structure with regions of substantial Li/Ni mixing. At slightly higher temperature, around ∼620 °C, the flower structures disintegrate and partially disorder to the honeycomb structure. Upon cooling, only the flower structure can be obtained.
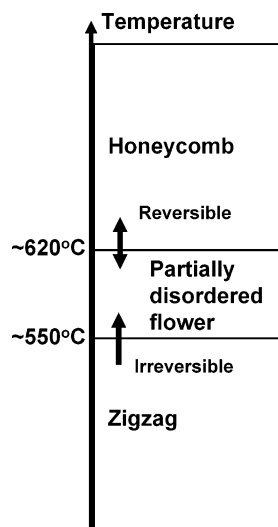
Figure 13. Schematic phase diagram of LiNi$_{0.5}$Mn$_{0.5}$O$_2$. The temperatures were obtained from Monte Carlo simulations.

Limitation of the Simulation. Finally, the limitations of our approach should be noted. Locally non-charge-balanced structures appear easily in MC simulations of LiNi$_{0.5}$Mn$_{0.5}$O$_2$, for example, in Figure 5. Because of our short-range cluster expansion, the electrostatic repulsion of locally charged regions is underestimated. If the structure is locally charge balanced, the electrostatic forces from relatively small regions decay rapidly, because the net charge of that small region is close to zero and multipole (dipole, quadrupole, and higher) terms dominate at longer ranges.[50] These multipole terms decay very quickly, making the cluster expansion applicable to such systems. However, for locally non-charge-balanced systems, the electrostatic forces extend to long range. Although the shorter-range part of that electrostatics is captured in the ECI, the longer-range part is not.

Conclusion

The cation ordering in LiNi$_{0.5}$Mn$_{0.5}$O$_2$ is a complex function of the temperature and the heating/cooling history. The zigzag model, which has very little Li/Ni disorder, is

the ground state of LiNi$_{0.5}$Mn$_{0.5}$O$_2$ in the GGA+U approach. We discussed, with underlying physics, a model that points out the phase transition upon heating in the LiNi$_{0.5}$Mn$_{0.5}$O$_2$ system and propose a phase diagram as shown in Figure 13. Zigzag ordering first transforms to a partially disordered flower structure, which upon further heating transforms to a disordered honeycomb structure. The cluster expansion and MC simulation of GGA+U energies match TEM, DSC, and XRD results along with previous NMR studies.[26] Once cation exchange between Li and TM layers occurs and Mn rings form around the Li in the TM layer, it is very difficult to break up the ring, which explains why states with low Li/Ni disorder cannot be obtained by cooling from high temperature. Therefore, it is crucial not to heat low Li/Ni disorder materials above a critical temperature at which Li/Ni exchange would occur. The unusual ordering of this material with temperature is due to the competition between electrostatics and Ni$_{TM}$−O−Ni$_{Li}$ hybridization.

Our work also illustrates how first principles modeling coupled with selected experiments can give insight into cation ordering in complex materials such as LiNi$_{0.5}$Mn$_{0.5}$O$_2$, which is a prerequisite to better understanding the structure−property relations.

(50) Ceder, G.; Garbulsky, G. D.; Tepesch, P. D. *Phys. Rev. B* **1995**, *51*, 11257.

(51) Izumi, F.; Dilanian, R. A. *IUCr Newslett.* **2005**, *32*, 59.